Acta Materialia 95 (2015) 335–342

Contents lists available at ScienceDirect

Acta Materialia

journal homepage: www.elsevier.com/locate/actamat

Structure evolution of soft magnetic $(Fe_{36}Co_{36}B_{19.2}Si_{4.8}Nb_4)_{100-x}Cu_x$ ($x = 0$ and 0.5) bulk glassy alloys

Mihai Stoica [a,b,*], Parthiban Ramasamy [a], Ivan Kaban [a], Sergio Scudino [a], Mircea Nicoara [b], Gavin B.M. Vaughan [c], Jonathan Wright [c], Ravi Kumar [d], Jürgen Eckert [a,e]

[a] IFW Dresden, Institute for Complex Materials, Helmholtzstr. 20, D-01069 Dresden, Germany
[b] POLITEHNICA University Timisoara, P-ta Victoriei 2, RO-300006 Timisoara, Romania
[c] European Synchrotron Radiation Facility (ESRF), F-38042 Grenoble, France
[d] Department of Metallurgical and Materials Engineering, Indian Institute of Technology Madras, 600036 Chennai, India
[e] TU Dresden, Institute of Materials Science, D-01062 Dresden, Germany

ARTICLE INFO

Article history:
Received 18 February 2015
Revised 21 May 2015
Accepted 27 May 2015
Available online 14 June 2015

Keywords:
Bulk metallic glasses
Synchrotron radiation
Thermal analysis
Phase transformation
Magnetic properties

ABSTRACT

Fully amorphous rods with diameters up to 2 mm diameter were obtained upon 0.5 at.% Cu addition to the $Fe_{36}Co_{36}B_{19.2}Si_{4.8}Nb_4$ bulk metallic glass. The Cu-added glass shows a very good thermal stability but, in comparison with the Cu-free base alloy, the entire crystallization behavior is drastically changed. Upon heating, the glassy $(Fe_{36}Co_{36}B_{19.2}Si_{4.8}Nb_4)_{99.5}Cu_{0.5}$ samples show two glass transitions-like events, separated by an interval of more than 100 K, in between which a bcc-(Fe,Co) solid solution is formed. The soft magnetic properties are preserved upon Cu-addition and the samples show a saturation magnetization of 1.1 T combined with less than 2 A/m coercivity. The relaxation behavior prior to crystallization, as well as the crystallization behavior, were studied by time-resolved X-ray diffraction using synchrotron radiation. It was found that both glassy alloys behave similar at temperatures below the glass transition. Irreversible structural transformations take place when approaching the glass transition and in the supercooled liquid region.
© 2015 Acta Materialia Inc. Published by Elsevier Ltd. This is an open access article under the CC BY-NC-ND license (http://creativecommons.org/licenses/by-nc-nd/4.0/).

1. Introduction

Ferromagnetic metallic glasses and the resulting nanocrystalline alloys, produced through crystallization of the corresponding glassy precursors, are the softest magnetic materials known so far [1]. Based on their unique magnetic properties, many products consisting of ferromagnetic metallic glasses such as for example anti-theft labels or highly efficient magnetic transformers are widely used [2,3]. Since the first ferromagnetic metallic glass Fe-C-P was found in 1967 [4], Fe- and (Fe,Co)-based alloys are regarded as attractive industrial alloys due to a relatively low price and simple routes for fabrication. In general, multi-component alloys require lower critical cooling rates for glass formation and promote the formation of bulk metallic glasses (BMGs). Together with their high strength and good corrosion resistance [5–8], ferromagnetic metallic glasses may have a good potential for application as advanced functional and structural materials. Within several new BMG families developed in the last decade, (Fe–Co)–Si–B–Nb glassy alloys play an important role because they combine high glass-forming ability (GFA) with good magnetic and mechanical properties [9]. It was shown that the best composition in this alloy family is the $Fe_{36}Co_{36}B_{19.2}Si_{4.8}Nb_4$ alloy, which may be cast as amorphous rods with a diameter up to 7 mm [10]. These BMGs can reach a compressive strength of 4000 MPa [11] and show a DC magnetization of 1.13 T [10]. It was demonstrated that at least in the case of Fe-based glassy ribbons with small contents of Nb, minor addition of Cu might be a good way to trigger nanocrystallization of Fe(Si), averaging out the magnetic anisotropy and therefore increasing the soft magnetic properties, similar as in case of FINEMET alloys [12]. However, the nanocrystallization provokes a serious embrittlement of the ribbons, which makes their handling difficult.

In the (Fe-Co)-B-Si-Nb bulk amorphous alloy system, several groups have tried to elucidate the influence of a minor addition of Cu on GFA, mechanical and magnetic properties of the resulting alloys. Jia et al. reported on the GFA of $(Fe_{36}Co_{36}B_{19.2}Si_{4.8}Nb_4)_{100-x}Cu_x$ (x = 0, 0.5, 0.6, 0.7 and 1.0) alloys [13]. It was found that upon 0.6 at.% Cu addition 1 cm long fully glassy rods with 4 mm diameter can be cast. Shen et al. established that *in situ* formation of (Fe,Co) and $(Fe,Co)_{23}B_6$ microcrystalline grains

* Corresponding author at: IFW Dresden, Institute for Complex Materials, Helmholtzstr. 20, D-01069 Dresden, Germany.
E-mail address: m.stoica@ifw-dresden.de (M. Stoica).

http://dx.doi.org/10.1016/j.actamat.2015.05.042
1359-6454/© 2015 Acta Materialia Inc. Published by Elsevier Ltd.
This is an open access article under the CC BY-NC-ND license (http://creativecommons.org/licenses/by-nc-nd/4.0/).

during the solidification process can improve the ductility of the $(Fe_{36}Co_{36}B_{19.2}Si_{4.8}Nb_4)_{99.75}Cu_{0.25}$ BMG composite [14]. Inoue et al. reported on the effect of crystallization of Fe–Co–B–Si–Nb–Cu glassy alloys on their soft magnetic properties by heat treatment [15]. In the case of $(Fe_{36}Co_{36}B_{19.2}Si_{4.8}Nb_4)_{98}Cu_2$ amorphous ribbons, we found that during the solidification process the primary crystalline phase is the o-$(Fe,Co)_3B$ metastable phase, which is replaced by α-(Fe,Co), $(Fe,Co)_{23}B_6$ and $(Fe,Co)_2B$ phases under slower cooling conditions [16]. The precipitation of α-(Fe,Co) is beneficial for the improvement of the soft magnetic properties of as-cast rods. However, further improvement of the mechanical properties of these glassy alloys, and particularly their plastic deformation, are necessary. In more recent studies [17] we have shown that the addition of 1–3 at.% Cu to the $Fe_{36}Co_{36}B_{19.2}Si_{4.8}Nb_4$ base alloy results in a fine nanocrystalline structure consisting of a mixture of different phases including α-(Fe,Co) and fcc-Cu. This mixture of different phases did not deteriorate the soft magnetic properties, but the composites were very brittle.

Motivated by these studies, we considered to add less than 1 at.% Cu to the $Fe_{36}Co_{36}B_{19.2}Si_{4.8}Nb_4$ base alloy (hereafter named BA_{100}). Due to the fact that a control of compositional variation of the Cu content in steps of 0.1 at.% would not be industrially viable, in this paper we consider only one Cu-containing composition, i.e. $BA_{99.5}Cu_{0.5}$. In a very recent work [18] we have shown that $BA_{99.5}Cu_{0.5}$ BMG samples exhibit significant plastic deformation under compressive loading and studied the changes induced by mechanical loading through *in situ* X-ray diffraction using synchrotron radiation. In the present work we discuss in detail the changes on GFA and on thermal stability as well as the *in situ* structural relaxation brought by the 0.5 at.% Cu addition to the base composition. Additionally, the DC magnetic properties are discussed.

2. Experimental procedure

Alloy ingots with composition $(Fe_{36}Co_{36}B_{19.2}Si_{4.8}Nb_4)_{99.5}Cu_{0.5}$ (at.%) were produced in argon atmosphere by induction-melting mixtures of pure Fe (99.9 mass%), Co (99.9 mass%), Si single crystal pieces (99.999 mass%), crystalline B (99.8 mass%), $Fe_{25}Nb_{75}$ eutectic pre-alloy (99.9 mass%) and Cu (99.9 mass%). The binary $Fe_{25}Nb_{75}$ pre-alloy was prepared previously in an arc-melter under a high-purity argon atmosphere (i.e. 99.998%). Pieces of the alloyed ingots were melted in quartz tubes and the melt was subsequently injected into a water-cooled copper mold under a high-purity argon atmosphere to produce rod-shaped specimens with 1 and 2 mm diameter and a length of 50 mm. The melting temperature of the alloys was carefully monitored by an infrared pyrometer.

The structure of the as-cast rods as well as their *in situ* relaxation and crystallization behavior was examined by X-ray diffraction (XRD) in transmission configuration using a high intensity monochromatic synchrotron radiation with an energy of 99.15 keV ($\lambda = 0.01249$ nm) at the ID11 beamline at ESRF Grenoble, France. Samples cut from rods with 1 or 2 mm diameter were crushed in small pieces and closed under vacuum in quartz capillary tubes and placed in a computer-controlled Linkam hot stage. Samples stemming from the 2 mm diameter rods were used for *in situ* continuous heating up to complete crystallization, while the relaxation studies were performed for 1 mm diameter samples. In the latter case, the samples were cyclically heated and cooled with 10 K/min in the beam. During the first step, the samples were heated up to a temperature approximately 30 K lower than the corresponding glass transition temperature, then cooled down close to room temperature (the second step), and heated above the crystallization temperature in the third step. In order to analyze the crystallization behavior, the samples were heated continuously with 10 K/min from room temperature to 1073 K. Prior to the heating experiments, the Linkam hot-stage was carefully calibrated by *in situ* checking the melting points of pure (minimum 99.9%) Sn, Zn, Al and Ge elements. The 10 K/min heating rate at which all heating experiments were performed was chosen due to technical considerations. The diffraction images were recorded with a 2D detector (FReLoN CCD camera) and further integrated with respect to the radial and azimuthal coordinates on the 2D detector using the FIT2D software [19] in order to obtain the diffraction patterns. During the integration the patterns were carefully corrected for dark current and background. The sample-to-detector distance was calibrated using LaB_6 and CeO_2 NIST standard powders. In order to facilitate the comparison and for better physical understanding, the diffracted intensity I is plotted further as a function of the wave vector $Q = (4\pi \sin\theta)/\lambda$, where θ is half of the scattering angle.

The thermal stability and the melting behavior of the specimens were evaluated by differential scanning calorimetry (DSC) at constant heating and cooling rates of 20 K/min. The viscosity in the supercooled liquid region of the BA_{100} and $BA_{99.5}Cu_{0.5}$ amorphous rods as a function of temperature was measured by parallel plate rheometry using a Perkin-Elmer TMA7 instrument (heating rate 20 K/min).

The room temperature *M-H* hysteresis loops were recorded using a physical property measuring system (PPMS) equipped with a vibrating sample magnetometer (VSM) head. The coercivity was directly measured using a Coercimat-type device under a DC magnetic field, which can be continuously changed from −250 mT to + 250 mT. The thermomagnetic curves were recorded from room temperature up to 973 K with a Faraday magnetometer equipped with a permanent magnet providing a magnetic field gradient. Additionally, the density of the specimens was evaluated by the Archimedes's method, using a computer controlled microbalance and dodecane ($C_{12}H_{26}$) as working liquid. The final values were obtained by averaging over 50 experimental values.

The accuracy of the experimental data lies within ± 2.5 K in the case of DSC measurements and thermomagnetic curves, ± 0.1 A/m for coercivity, ± 80 A/m (i.e. ~1 Oe) for VSM measurements and 0.5% for density measurements. In the case of synchrotron XRD the maximum value for the wave vector Q was set to 100 nm^{-1}. Accordingly, an accidental shift of the sample position with 0.1 mm along the beam direction would result in a shift by 0.006 nm^{-1} for the maxima centered around 31 nm^{-1} and 0.01 nm^{-1} for the maxima centered around 52 nm^{-1}. The XRD and DSC results proved that the 1 mm and 2 mm diameter rod samples are structurally identical, i.e. fully amorphous, and the glass transition, crystallization and meting events take place at the same temperatures (within the measurement errors).

3. Results and discussion

3.1. Thermal stability and in situ structural evolution

Fig. 1 compares the DSC thermograms for BA_{100} and $BA_{99.5}Cu_{0.5}$ amorphous rods with 2 mm diameter. The melting behavior is affected by the addition of 0.5 at.% Cu: an extra endothermic event can be observed, but both alloys are off-eutectic and melt within the same range of temperatures. Interestingly, the lower temperature behavior is drastically changed. The base BMG undergoes clearly a glass transition event with onset at 826 K, followed by the supercooled liquid region (SLR) and crystallization, which starts at 869 K. Furthermore, two other small exothermic peaks can be observed. This type of alloy forms only one complex phase

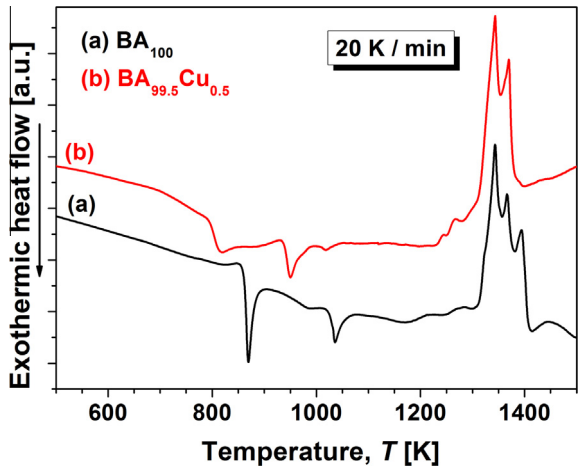

Fig. 1. DSC traces of BA_{100} and $BA_{99.5}Cu_{0.5}$ amorphous rods with 2 mm diameter, measured with 20 K/min constant heating rate (base lines not subtracted).

of the $Fe_{23}B_6$ type [17,20,14,21] by primary crystallization. The other peaks are associated to the final transformation of the residual amorphous matrix. In the case of the Cu-containing alloy, a glass transition-like event still can be observed, which is shifted towards lower temperatures. A large exothermic transformation centered at 838 K, which in other Cu-substituted alloys was associated to the nanocrystallization process [22], follows. Another glass transition-like event and subsequently a pronounced crystallization peak can be observed. Nevertheless, this apparent endothermic phenomenon currently attributed to a second glass-transition could result upon superposition of another exothermic event- as for example a crystallization with a small heat effect. The crystallization peak centered around 944 K has the tendency to broaden towards higher temperatures. Then, immediately above 1015 K, a last small exothermic event can be detected, most probably indicating complete crystallization of the remaining amorphous matrix. At approximately 1280 K, a kind of double endothermic event is present, which is not so apparent in the case of the BA_{100} sample. This last endothermic event prior to melting may indicate an allotropic transformation, as for example a bcc-to-fcc transition of the α-Fe-type solid solution.

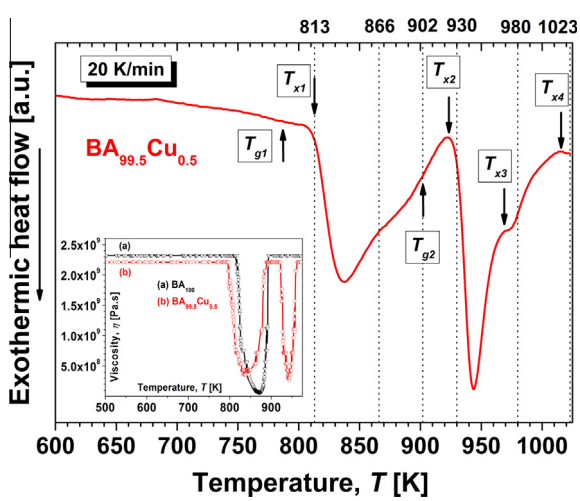

Fig. 2. DSC traces (base line subtracted) of the $BA_{99.5}Cu_{0.5}$ amorphous rod samples with 2 mm diameter. The characteristic temperatures are illustrated with bold characters. The inset displays the variation of the viscosity as a function of temperature, clearly proving that the Cu-added sample shows two supercooled liquid regions.

For clarity, Fig. 2 shows the DSC traces of the $BA_{99.5}Cu_{0.5}$ amorphous rod samples with 2 mm diameter only at lower temperatures and with the base line subtracted. The characteristic temperatures are marked in the figure and the notations are the usual ones: T_g stands for the glass transition temperature and T_x for the crystallization temperature. All temperatures were determined as the onset of the corresponding events using the two-tangent method. The values for both BA_{100} and $BA_{99.5}Cu_{0.5}$ amorphous samples are summarized in Table 1. In order to study the crystallization sequence in detail, selected XRD patterns are plotted in Fig. 3. In order to correlate the diffraction data with the DSC thermograms, the temperatures corresponding to each pattern are marked with dotted vertical lines in Fig. 2. A detail of the continuous evolution of the structure between 794 K and 910 K is further provided in Fig. 4. The structural changes, which can be easily observed in the corresponding XRD patterns presented in Fig. 3, can be correlated straightforward with the thermal behavior. At room temperature the as-cast sample is fully amorphous. Once the sample reaches T_{x1} (813 K) the crystallization starts, but a relatively long time would be needed for complete crystallization. The first broad diffraction peak characteristic of glassy materials is still present, which indicates that still some amorphous matrix has not yet transformed and/or the crystallized products are in the nm-range. The incipient Bragg peaks can be attributed to the bcc-(Fe,Co) solid solution. Most probably the low level of Cu, assisted by the positive heat of mixing between Cu and Fe [23], promotes the primary nanocrystallization of the bcc solid solution. At 866 K and 902 K, i.e. below and at the slightly endothermic event having its onset at T_{g2} = 902 K (i.e., an event associated most probably with the glass transition of the remaining amorphous matrix) the structure of the sample consists of only bcc-(Fe,Co) solid solution along with the residual amorphous matrix. Judging from the relative intensities and the shape of the peaks (for clarity see Fig. 4) it can be assumed that at 902 K the sample contains a larger amount of bcc-(Fe,Co) solid solution than at 866 K. This is consistent with the DSC thermograms, in which the first crystallization event extends over 100 K. As mentioned in the experimental part, due to technical limitations the continuous *in situ* heating was performed at 10 K/min, i.e. a heating rate lower than the 20 K/min used for the DSC measurements. It is known that at lower heating rates the main temperatures may shift towards lower values [20]. Accordingly, the DSC temperatures marked in Fig. 2 might not correspond directly to those marked in Fig. 3. This is equivalent with the consideration that the XRD patterns from Fig. 3 reveal the actual structure at a *slightly higher* temperature than those indicated in the figure. Moreover, this proves the thermal stability of the sample. Furthermore, the patterns presented in Fig. 4 start in the supercooled liquid region (SLR) of the initially fully amorphous and homogeneous (as proved by XRD measurements, see Fig. 3) BMG sample and finish within the supercooled liquid region of the remaining amorphous matrix. The crystalline peaks superimposed on the amorphous broad maxima are characteristic only for a bcc-(Fe,Co) solid solution. Nevertheless, 902 K is a very high temperature for a glass transition and with 108 K above the first glass transition temperature.

Table 1
Characteristic temperatures of the as-cast BA_{100} and $BA_{99.5}Cu_{0.5}$ BMG rods with 2 mm diameter: T_g stands for the glass transition event(s), while T_x refers to the crystallization event(s). For details see Fig. 2.

	T_g	T_x				
Temperature [K] BA_{100} alloy	826	869				
	T_{g1}	T_{x1}	T_{g2}	T_{x2}	T_{x3}	T_{x4}
Temperature [K] $BA_{99.5}Cu_{0.5}$ alloy	794	813	902	929	975	1015

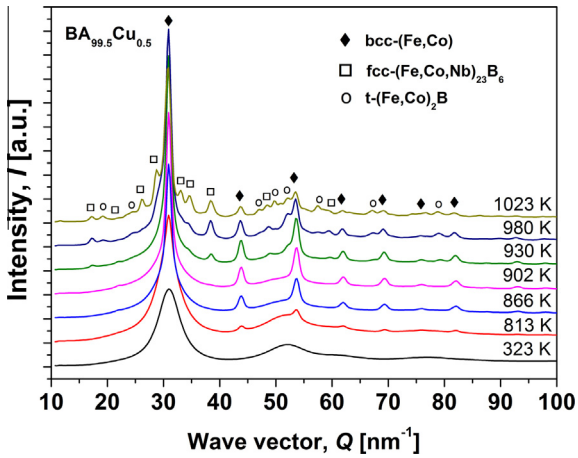

Fig. 3. XRD patterns for $BA_{99.5}Cu_{0.5}$ amorphous rod samples with 2 mm diameter at different temperatures. The corresponding temperatures are marked with dotted lines in Fig. 2. The patterns were measured in transmission configuration using synchrotron radiation upon *in situ* continuous heating.

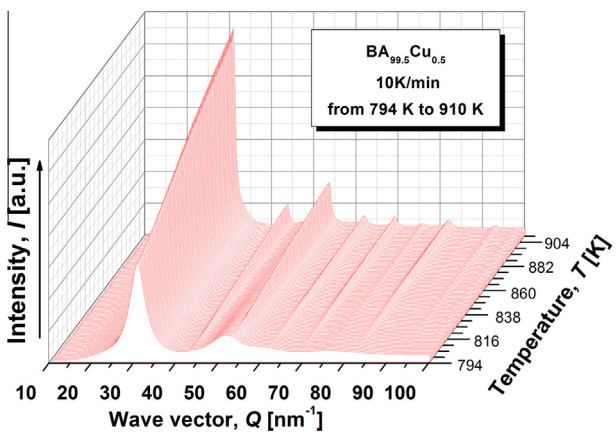

Fig. 4. Detail of the continuous evolution of the structure between 794 K and 910 K measured *in situ* for a $BA_{99.5}Cu_{0.5}$ amorphous rod samples with 2 mm diameter.

However, a glass transition at 902 K is not exotic: several Fe-based glasses containing Nb show very high glass transition temperatures, close or even above 900 K [24]. As mentioned before and seen especially in Fig. 4, the amount and/or dimensions of the (Fe,Co) solid solutions crystallites increase gradually and, as a consequence, the composition of the residual matrix changes continuously. In this way it becomes strongly enriched in Nb, as well as in B and Si, and this may increase its stability against crystallization, thus leading to a higher glass transition temperature.

If one assumes that the presence of Cu may provoke clustering of (Fe,Co) atoms upon casting, then at the early stages the primary precipitation proceeds through fast nucleation. For further growth of the nanocrystals diffusion processes over longer distances are necessary, which require time. Due to the primary crystallization, the composition of the remaining amorphous matrix changes continuously as the (Fe,Co) crystals grow. To clarify this aspect, the influence of temperature on the viscosity of the as-cast BA_{100} and $BA_{99.5}Cu_{0.5}$ amorphous samples was studied by parallel plate rheometry (see the inset in Fig. 2). For these measurements, small slices cut from 2 mm diameter rods were carefully plan-parallel polished. However, the aspect ratio of the samples, i.e. the height h to radius r ratio, was in our case larger than 0.25, the value up to which Stefan's equation can be applied without corrections [25–27]. Instead, the viscosity η was calculated taking into account the change of the height of the sample versus time, as well as of the volume:

$$\eta = -\frac{2\pi F h^5}{3V^2\left(\frac{dh}{dt}\right)}, \quad (1)$$

where F is the applied load (i.e. 2.6 N) and V is the volume of the sample. This allows viscosity measurements in the range from 10^5 to 10^{11} Pa s [25–27].

In the case of the BA_{100} sample, the viscosity starts to decrease at the onset of the glass transition temperature (i.e. 826 K), dropping from 2.3×10^9 to 10^7 Pa s. As seen in Fig. 1, the crystallization finishes slightly before 900 K. At this temperature the viscosity recovers its initial higher value (see the inset in Fig. 2). As mentioned in previous works [20], the base alloy forms only one complex phase of the $Fe_{23}B_6$ type by primary crystallization. Moreover, the crystallization proceeds with a very short incubation time, but for complete crystallization a long time is required [20]. The viscosity drop presented in the inset in Fig. 2 follows this trend: the viscosity drops at T_g and increases again when the exothermic event associated with primary crystallization sets in.

For $BA_{99.5}Cu_{0.5}$ amorphous samples, the viscosity decreases with increasing temperature from about 2.2×10^9 Pa s at 700 K to 3×10^8 Pa s at 832 K, which indicates as well the occurrence of a glass transition and the transformation of the glassy solid into the supercooled liquid. Above 832 K the viscosity starts to increase with increasing temperature, indicating the loss of liquid-like behavior. However, the increase is not abrupt and this is consistent with the broad first exothermic event observed in the DSC. Above 900 K, a second drop of viscosity is visible, and with further temperature increase it decreases from about $2.2 \cdot 10^9$ Pa s to $2.5 \cdot 10^8$ Pa s at 944 K. This clearly indicates the occurrence of a second glass transition, characteristic to the remaining amorphous matrix. The peak temperatures of the viscosity minima (832 K and 944 K) match almost perfectly the peak temperatures of the crystallization events as seen in the DSC (838 K and 944 K), while the temperatures where the viscosity starts to decrease seem to be shifted towards higher temperatures when compared with the DSC thermograms. This is just a measurement artifact and can be explained if one assumes that the fast succession of the endothermic glass transition and the exothermic crystallization events cannot be strictly followed by the device. Moreover, the TMA measures the temperature of the heater and not directly the sample temperature.

For the $BA_{99.5}Cu_{0.5}$ sample, at 930 K, i.e. immediately above the second crystallization step (Fig. 2), new crystalline peaks attributed to an fcc $(Fe,Co,Nb)_{23}B_6$-type phase appear, which coexists with the bcc (Fe,Co) solid solution (Fig. 3). Further heating to 980 K, i.e. a temperature above the small exothermic event superimposed on the second crystallization peak and which is considered here the third crystallization step, causes the appearance of new peaks in the XRD pattern, which can be attributed to the equilibrium tetragonal phase $(Fe,Co)_2B$. The first broad peak can be seen even after heating the sample up to 930 K, which may indicate the presence of a residual amorphous matrix. At 1015 K (see Figs. 1 and 2) an extra small exothermic event might be present. The XRD pattern for the sample annealed at 1023 K clearly shows an increased amount of the $(Fe,Co)_2B$ phase coexisting with the (Fe,Co) solid solution and the $(Fe,Co,Nb)_{23}B_6$-type phase.

Taking into account all experimental findings, the evolution of the structure of the $BA_{99.5}Cu_{0.5}$ BMGs can be summarized as follows: amorphous phase 1 → amorphous phase 2 + (Fe,Co) → residual amorphous phase (eventually) + (Fe,Co) + $(Fe,Co,Nb)_{23}B_6$ → (Fe,Co) + $(Fe,Co,Nb)_{23}B_6$ + $(Fe,Co)_2B$. This sequence is completely different from the one found for the base alloy [20], in which the amorphous sample transforms almost completely through a single sharp crystallization event into the $(Fe,Co,Nb)_{23}B_6$ phase (see also Fig. 1). However, there remains a small volume fraction of a residual amorphous matrix, which crystallizes after a large

temperature interval (i.e. 120 K) into a mixture of the equilibrium tetragonal $(Fe,Co)_2B$ phase and metastable orthorhombic $(Fe,Co)_3B$. The differences in the crystallization behavior are certainly linked to the different atomic arrangements in the two types of amorphous alloy samples. Therefore, it is reasonable to expect different macroscopic properties.

3.2. In situ studies of structure relaxation prior crystallization

We have recently shown that the $BA_{99.5}Cu_{0.5}$ amorphous rods with 1 mm diameter can undergo a compressive plastic deformation up to 3.8% strain at fracture (for additional details see [18]). This is an important finding, because the usual brittleness of soft ferromagnetic BMGs may hinder their application. The Fe-based BMGs, despite being very strong, may break directly upon casting if one tries to use molds with complex geometries [28]. Improving the plastic deformation is in this case associated with the need for casting samples with adequate geometries for direct use as magnetic parts, rather than to the idea of making the Fe-based BMGs suitable for structural applications. It was found [18] that upon compression tests, despite numerous serrations in the stress–strain curve and 1.5% pure plastic strain, the samples do not deform as expected, i.e. via extensive shear band creation. However, there are indications that some layers have flowed and this phenomenon took place before the brittle final fracture. The overall performance and the macroscopic plastic strain depend on the interaction between cleavage-like and viscous flow-like features. Further *in situ* compression tests using synchrotron radiation provided enough reasons to conclude that such fracture mechanisms may be explained by different mechanical behavior of different neighborhood atomic shells [18].

Here, through time-resolved XRD using synchrotron radiation, we provide evidence for the structural transformation behavior upon thermal cycling before the glass transition. The room temperature XRD patterns using monochromatic synchrotron radiation, for both as-cast BA_{100} and $BA_{99.5}Cu_{0.5}$ rods with 1 mm diameter, are presented in Fig. 5. The patterns show only diffuse maxima, as it is characteristic for amorphous materials. The main, the second and the third (i.e. the shoulder) broad maxima, marked in the figure and usually named Q_1, Q_2 and Q_3 are centered at $Q_1 = 31.039\ nm^{-1}$, $Q_2 = 51.918\ nm^{-1}$ and $Q_3 = 60.143\ nm^{-1}$ in the case of BA_{100}, and at $Q_1 = 31.117\ nm^{-1}$, $Q_2 = 52.22\ nm^{-1}$ and $Q_3 = 60.63\ nm^{-1}$ in the case of $BA_{99.5}Cu_{0.5}$. The Q positions were obtained upon fitting the XRD patterns using a pseudo-Voigt function. The fitting errors are $\pm 0.003\ nm^{-1}$ for Q_1, $\pm 0.02\ nm^{-1}$ for Q_2 and $\pm 0.07\ nm^{-1}$ for Q_3, which are comparable with the absolute errors (i.e. ± 0.006, ± 0.01 and ± 0.02 nm^{-1}, respectively) introduced by the uncertainties in determining the sample-to-detector distance. It can be observed that the fitting errors tend to become larger for larger Q. This is why only Q_1 and Q_2 will be considered for further thermal analysis.

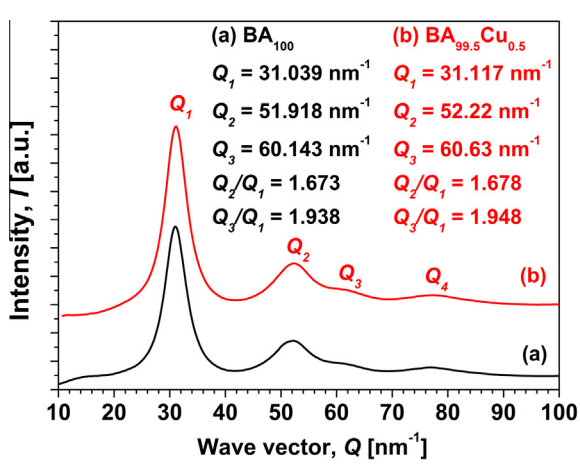

Fig. 5. Room temperature XRD patterns collected using monochromatic synchrotron radiation, for both as-cast BA_{100} and $BA_{99.5}Cu_{0.5}$ rods with 1 mm diameter.

Comparing the positions of the first, second and third maxima for as-cast BA_{100} and $BA_{99.5}Cu_{0.5}$ samples one can notice that they are slightly changed, the differences being in any case at least one order of magnitude larger than the absolute errors. However, for both glassy samples the ratio of the Q_2/Q_1 is almost the same (1.673 for BA_{100} and 1.678 for $BA_{99.5}Cu_{0.5}$, see Fig. 7), as well as Q_3/Q_1 (1.938 for BA_{100} and 1.948 for $BA_{99.5}Cu_{0.5}$). These values are in good agreement and extremely close to those predicted for a perfect icosahedron ($Q_2/Q_1 = 1.7$ and $Q_3/Q_1 = 2.0$) [29,30], indicating that both glassy samples with different chemical compositions have a similar topological short-range order (SRO) characterized by strong indications for icosahedral arrangement.

The *in situ* XRD using synchrotron radiation is nowadays an established method to investigate the structural changes in metallic glasses when resolution in the range of seconds is required [31–33]. Many details may be obtained even directly from analyses in the reciprocal space, for example by studying the changes in the peak positions, intensity and/or full width at half maximum induced by temperature variations. Fig. 8(a) and (b) shows the behavior of the first two maxima Q_1 and Q_2: (a) for a BA_{100} sample and (b) for a $BA_{99.5}Cu_{0.5}$ sample upon cyclic heating. For clarity Q_2 is shifted down by 20.6 nm^{-1} for th BA_{100} sample and by 20.8 nm^{-1} for the $BA_{99.5}Cu_{0.5}$ sample. The glass transition and crystallization temperatures are indicated by vertical lines and the experimental data finish in the vicinity of the corresponding crystallization temperatures. In both cases, the deviation from linearity above T_g and prior T_x is due to entering into the SLR. The positions of the diffraction peaks follow the thermal cycle procedure, i.e. heating–cooling-heating. During heating, the positions of the Q_1 and Q_2 maxima shift towards smaller values, indicating an expansion of the interatomic distances (because the Q-values in the reciprocal space scale inversely proportional with the distances in the real space), and upon cooling they shift towards higher values. For both alloys, Q_1 and Q_2 shift in the same direction before entering into the SLR, but the slopes of $Q_{1,2}(T)$ are different. Once above T_g the behavior drastically changes: the BA_{100} sample shows an increase of the mean interatomic distance, while the $BA_{99.5}Cu_{0.5}$ sample seems to become more dense. This can be explained if one assumes that the Fe atoms starts to cluster and the chemical composition of the matrix changes continuously. Such behavior is in agreement with the data presented in Figs. 2 and 4.

Yavari et al. [32] have shown that when approaching the glass transition temperature, the free volume which may be present in a glassy sample is annealed out. This would mean that when approaching the glass transition the position of Q_1 would shift faster towards lower values. As a consequence, if the temperature is further decreased (the sample being still amorphous but sub-T_g annealed) and then a second heating follows, one should notice that the Q_1 variation follows the same curve upon cooling-second heating, but should be different from the one observed during the first heating (for details see reference [32]). More recently, Mattern et al. [33] have concluded that such analysis is not always accurate, since the samples are prone to irreversible structural transformations, i.e. changes in the atomic arrangement. In Fig. 6(a), as well as in Fig. 6(b), one can clearly see that there are no differences in behavior upon cyclically heating for our samples. The variation of both Q_1 and Q_2 follows the same curves with the same slopes, observable differences being visible only very immediately before the glass transition. However, the behavior in the

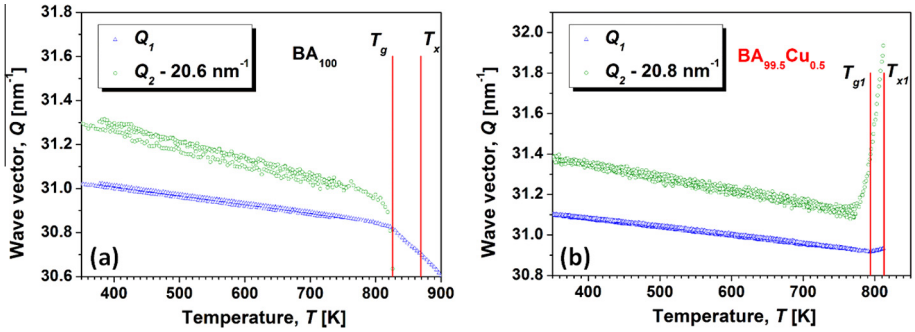

Fig. 6. Behavior of the first two maxima Q_1 and Q_2 for BA_{100} (a) and $BA_{99.5}Cu_{0.5}$ (b) samples measured upon cyclic heating. For clarity Q_2 is shifted down by 20.6 nm^{-1} for the BA_{100} sample and by 20.8 nm^{-1} for the $BA_{99.5}Cu_{0.5}$ sample. In both cases the corresponding glass transition and crystallization temperatures are marked by vertical lines.

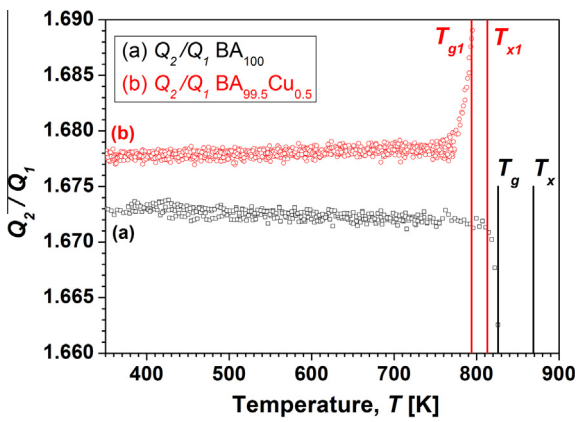

Fig. 7. Peak position ratio for BA_{100} (curve a) and $BA_{99.5}Cu_{0.5}$ (curve b) samples as a function of temperature. The corresponding glass transition and crystallization temperatures are marked by vertical lines.

immediate vicinity of the glass transition and further in the SLR is drastically changed: for the BA_{100} sample the Q_1 and Q_2 values decrease continuously, faster than before T_g, while for the $BA_{99.5}Cu_{0.5}$ sample they increase. In the case of the BA_{100} sample this means expansion of the interatomic distances, as it would be expected to happen when the temperature increases. For the $BA_{99.5}Cu_{0.5}$ sample it seems that the distances between the atoms shrink immediately before and after the glass transition and, due to the differences in slopes (i.e. Q_2 shifts with a much larger slope than Q_1), the nearest neighbors move over larger distances when

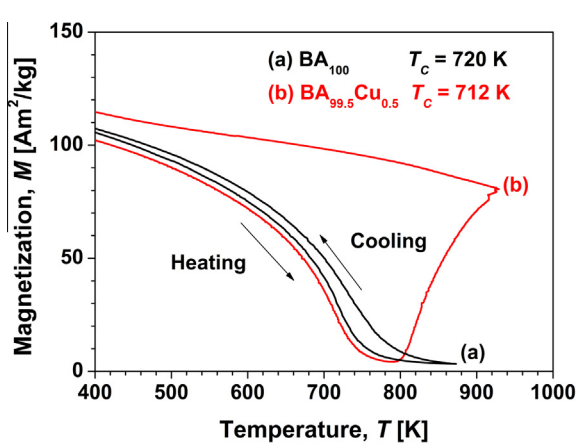

Fig. 8. Variation of saturation magnetization with temperature for both BA_{100} and $BA_{99.5}Cu_{0.5}$ amorphous rod samples with 2 mm diameter.

compared with the average interatomic distances. Again, such behavior can be explained if one assumes that the Fe atoms started to migrate and cluster and the chemical composition of the amorphous matrix changes continuously, in perfect agreement with the DSC, viscosity and XRD data.

For crystalline materials, the linear thermal expansion coefficient α of an interatomic spacing r_i can be calculated from the slope [33]

$$\frac{\partial Q_i(T)}{\partial T} = -\frac{\partial r_i(T)}{\partial T} = -\alpha Q_i \tag{2}$$

because $Q_i = 2\pi/r_i$. In the case of amorphous alloys, assuming that the Ehrenfest equation $Q_i = 1.23 \times (2\pi/r_i)$ [34] can be applied, the values of the thermal expansion coefficient α estimated from the slope of the corresponding Q_1 plots are $1.29 \times 10^{-5}\ K^{-1}$ for BA_{100} sample and $1.33 \times 10^{-5}\ K^{-1}$ for $BA_{99.5}Cu_{0.5}$ sample. Both values are very close, indicating a similar behavior, and comparable with other values reported in literature [32,33].

The scattered intensity of a glass $I(Q)$ can be calculated using Debye's equation [35]:

$$I(Q) = \sum f_i f_j \frac{\sin Q r_{ij}}{Q r_{ij}}, \tag{3}$$

which is the sum over all interatomic distances r_{ij} of n atoms multiplied by the atom form factors f_i of the atoms ($i, j = 1 \ldots n$). In crystalline materials, the thermal volume expansion is usually accompanied with an increase of the unit cell and correspondingly of all interatomic distances. If all interatomic distances r_{ij} increase with temperature by the same factor k, i.e. $r_{ij}(T) = r_{ij}(1 + \alpha \cdot \Delta T) = k \cdot r_{ij}$, the scattered intensity $I^*(Q/k)$ is equal to $I(Q)$ [33]. This means that all maxima positions Q_i^* of the scattering functions of $I^*(Q)$ are decreased by a factor $1/k$. If this is valid for the thermal expansion of a metallic glass, or in other words if a metallic glass expands isotropically, the ratio of any diffraction maxima positions has to be constant for different temperatures. If one assumes that the metallic glasses can be described by a hard-sphere model [36], the positions of the broad maxima are mostly related to the different neighborhood shells. If the neighborhood shells have the same stiffness, they should thermally expand in the same way and the ratio of any diffraction maxima positions should be always constant. Fig. 7 shows the peak position ratio for BA_{100} (curve a) and for $BA_{99.5}Cu_{0.5}$ samples (curve b). It is seen that at the temperatures below T_g the ratio Q_2/Q_1 is virtually constant. However, once approaching the glass transition there are major differences between the two alloys, which follow the trend observed in Fig. 6(a) and (b). Most probably there is a topological atomic rearrangement brought by the thermal activation and favored by different stiffness of different atomic shells. The actual experimental data complete our latest results [18] obtained by *in situ* compression

tests and together with similar works may provide a more complete image on the effect of Cu additions to the base compositions.

3.3. DC Magnetic properties

Fig. 8 shows the thermomagnetic curves for BA_{100} and $BA_{99.5}Cu_{0.5}$ amorphous rod samples with 2 mm diameter. For temperatures close to T_C, the saturation magnetization M_S can be described by [37]:

$$M_S(T) = M(0)\left(1 - \frac{T}{T_C}\right)^{\beta}, \quad (4)$$

with the exponent $\beta = 0.36$. In order to minimize the errors, the experimental results were separately plotted as $(M_S)^{1/\beta}$ versus T (not presented here). Then the Curie temperature was considered as the temperature were the $(M_S)^{1/\beta}$ deviates from linearity. The base alloy shows a Curie temperature of 720 K, while it decreases to 712 K. However, this decrease by only 8 K upon Cu addition is very small. More interesting is the variation of the magnetization with temperature. There one can see that in the case BA_{100} alloy, which has a crystallization temperature $T_x = 869$ K [20], the first phase which crystallizes is either nonmagnetic or has the corresponding Curie temperature lower than T_x. This confirms in fact the previous findings about the formation of the $Fe_{23}B_6$-type phase, because this phase is magnetic, its Curie temperature depending strongly on the content of magnetic atoms (the real composition is $(Fe,Co,Nb)_{23}B_6$) but being lower than 869 K [20]. As it was shown previously (see Figs. 1–3), the $BA_{99.5}Cu_{0.5}$ glass has the onset of the first crystallization event at 813 K and the primary precipitated phase is bcc (Fe,Co). This is in perfect agreement with the thermomagnetic behavior shown in Fig. 8, where one can clearly see that the crystallized phase has a high Curie temperature, impossible to be revealed by the current curve due to the technical limitation. Moreover, the saturation magnetization at 400 K (and implicitly at room temperature), which is slightly lower compared to BA_{100} BMG, becomes larger after cooling due to the presence of the crystalline bcc (Fe,Co) in ferromagnetic state.

Fig. 9 shows comparison of the hysteresis curves for both BA_{100} and $BA_{99.5}Cu_{0.5}$ BMG samples with 2 mm diameter. As observed upon thermomagnetic investigation, the saturation magnetization of the Cu-containing amorphous alloy (110 Am^2/kg measured at room temperature by VSM) is just slightly lower than that of base alloy (113 Am^2/kg, measured in the same conditions). Both alloys show almost zero remanence magnetization and less than 2 A/m coercive field, as measured by a coercimat. The density of the base alloy was measured to be $\rho = 7768$ kg/m^3 and the alloy with 0.5% Cu addition has $\rho = 7752$ kg/m^3, values which, within the measurement errors (i.e. 0.5%), are almost the same. Then, the saturation polarization calculated as $J_s = 4\pi 10^{-7}\rho M_S$ is for both alloys around 1.1 T, a value which, together with the very small coercivity and zero remanence, makes the alloys very attractive for applications as soft magnetic material. In conclusion, the 0.5 at.% Cu addition does not affect the room temperature soft magnetic behavior, and, as recently shown [18], it improves the mechanical behavior considerably.

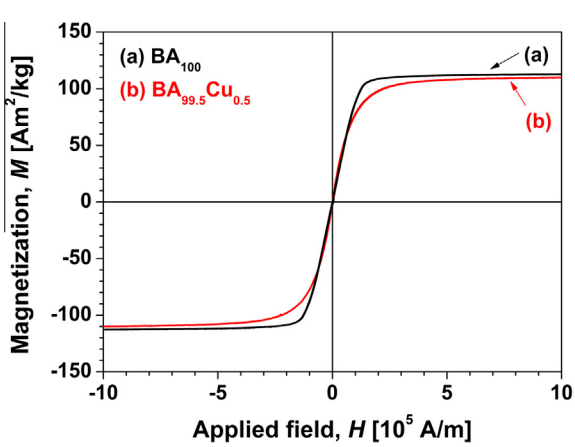

Fig. 9. Hysteresis curves for both BA_{100} and $BA_{99.5}Cu_{0.5}$ BMG rod samples with 2 mm diameter.

4. Conclusions

The addition of only 0.5 at.% Cu to the base $Fe_{36}Co_{36}B_{19.2}Si_{4.8}Nb_4$ glassy alloys drastically changes the crystallization behavior. Amorphous rods cast using the new alloy composition show very good soft magnetic properties: 1.1 T saturation, less than 2 A/m coercivity, and 712 K Curie temperature. The variation of the saturation magnetization with temperature is in perfect agreement with the crystallization behavior as observed by calorimetric studies. Altogether these values make the glassy samples attractive for magnetic applications. *In situ* synchrotron studies have shown that the two alloys, upon a heating–cooling-heating sub-T_g thermal cycle, suffer irreversible transformation at the glass transition temperature. In the SLR the positions of the broad diffraction maxima shift towards smaller values in the case of the base alloy and towards larger values for the Cu-added alloy.

Acknowledgements

The authors thank N. Mattern for fruitful discussions, as well as B. Bartusch, M. Frey and S. Donath for technical assistance. Dr. Jozef Bednarčik from DESY is specially acknowledged for the help with data evaluation and valuable discussions. The work has been done in the frame of the ERC Advanced Grant INTELHYB (Grant agreement no.: 340025). The partial support of the German Science Foundation (DFG) through the grant STO 873/2, as well as the support of the ESRF through the projects HD 613 and HC 1178 is fully acknowledged. P.R. and M.N. acknowledge the financial support of the German Academic Exchange Service (DAAD).

References

[1] G. Herzer, Nanocrystalline soft magnetic alloys, in: K.H.J. Bushow (Ed.), Handbook of Magnetic Materials, vol. 10, Elsevier Science B.V., 1997.
[2] Y. Yoshizawa, K. Yamauchi, IEEE Trans. Magn. 25 (1989) 3324.
[3] <http://www.sensormatic.com/Products/EAS/Labels/Labels_home.aspx>.
[4] P. Duwez, S.C.H. Lin, J. Appl. Phys. 38 (1967) 4096.
[5] A. Inoue, Y. Shinohara, J.S. Gook, Mater. Trans. JIM 36 (1995) 1427.
[6] A. Inoue, T. Zhang, A. Takeuchi, Appl. Phys. Lett. 71 (1997) 464.
[7] M. Stoica, J. Eckert, S. Roth, Z.F. Zhang, L. Schultz, W.H. Wang, Intermetallics 13 (2005) 764.
[8] T. Zhang, F.J. Liu, S.J. Pang, R. Li, Mater. Trans. 48 (2007) 1157.
[9] B.L. Shen, A. Inoue, C. Chang, Appl. Phys. Lett. 85 (2004) 4911.
[10] T. Bitoh, A. Makino, A. Inoue, A.L. Greer, Appl. Phys. Lett. 88 (2006) 182510.
[11] A. Inoue, B.L. Shen, C.T. Chang, Acta Mater. 52 (2004) 4093.
[12] Y. Yoshizawa, S. Oguma, K. Yamauchi, J. Appl. Phys. 64 (1988) 6044.
[13] Y. Jia, S. Zeng, S. Shan, L. Zhang, C. Fan, B. Zhang, B. Zhan, R. Liu, W. Wang, J. Alloys Compd. 440 (2007) 113.
[14] B.L. Shen, H. Men, A. Inoue, Appl. Phys. Lett. 89 (2006) 101915.
[15] A. Inoue, B.L. Shen, J. Mater. Res. 18 (2003) 2799.
[16] R. Li, M. Stoica, J. Eckert, J. Phys. Conf. Ser. 144 (2009) 012042.
[17] M. Stoica, R. Li, S. Roth, J. Eckert, G. Vaughan, A.R. Yavari, Met. Mater. Trans. A 42 (2011) 1476.
[18] M. Stoica, S. Scudino, S. Bednarčik, I. Kaban, J. Eckert, J. Appl. Phys. 115 (2014) 053520.
[19] A.P. Hammersley, S.O. Svensson, M. Hanfland, A.N. Fitch, D. Haeusermann, High Press. Res. 14 (1996) 235.
[20] M. Stoica, R. Li, A.R. Yavari, G. Vaughan, J. Eckert, N. Van Steenberge, D. Ruiz Romera, J. Alloys Compd. 504 (2010) S123.
[21] R. Li, S. Kumar, S. Ram, M. Stoica, S. Roth, J. Eckert, J. Phys. D: Appl. Phys. 42 (2009) 085006.
[22] J.M. Borrego, C.F. Conde, A. Conde, M. Stoica, S. Roth, J.M. Greneche, J. Appl. Phys. 100 (2006) 043515.

[23] F.R. De Boer, R. Boom, W.C.M. Mattens, A.R. Miedema, A.K. Niessen, Cohesion in Metals, Elsevier Science Publishing Company Inc., North Holland Amsterdam, 1989.
[24] J.M. Park, J.S. Park, J.H. Na, D.H. Kim, D.H. Kim, Mater. Sci. Eng. A 435–436 (2006) 425.
[25] G.J. Dienes, H.F. Klemm, J. Appl. Phys. 17 (1946) 458.
[26] E. Bakke, R. Busch, W.L. Johnson, Appl. Phys. Lett. 67 (1995) 3260.
[27] S. Scudino, B. Bartusch, J. Eckert, J. Phys. Conf. Series 144 (2009) 012097.
[28] A. Bárdos, A. Lovas, S. Roth, M. Stoica, L.K. Varga, Czech. J. Phys. 55 (2005) 593.
[29] S. Sachdev, D.R. Nelson, Phys. Rev. Lett. 53 (1984) 1947.
[30] K.F. Kelton, G.W. Lee, A.K. Gangopadhyay, R.W. Hyers, T.J. Rathz, J.R. Rogers, M.B. Robinson, D.S. Robinson, Phys. Rev. Lett. 90 (2003) 195504.
[31] N. Mattern, U. Kühn, H. Hermann, S. Roth, H. Vinzelberg, J. Eckert, Mater. Sci. Eng. A 375–377 (2004) 351.
[32] A.R. Yavari, A. Le Moulec, A. Inoue, N. Nishiyama, N. Lupu, E. Matsubara, et al., Acta Mater. 53 (2005) 1611.
[33] N. Mattern, M. Stoica, G. Vaughan, J. Eckert, Acta Mater. 60 (2012) 517.
[34] P. Ehrenfest, Proc Koninklijke Akademie van Wetenschappen Amsterdam 17 (1915) 1184.
[35] P. Debye, Annalen der Physik 46 (1915) 809.
[36] J.D. Bernal, Nature 185 (1960) 68.
[37] G. Herzer, IEEE Trans. Magn. 25 (1989) 3327.